ELSEVIER

Journal of Molecular Catalysis A: Chemical 118 (1997) 101–111

JOURNAL OF MOLECULAR CATALYSIS A: CHEMICAL

Support effect on the formation of the well-defined PtSn alloy from a Pt–Sn bimetallic complex. Catalytic properties in the activation of CO_2

Jordi Llorca [a], Pilar Ramírez de la Piscina* [a], José-Luis G. Fierro [b], Joaquim Sales [a], Narcís Homs [a,*]

[a] *Departament de Química Inorgànica. Universitat de Barcelona. Diagonal 647., 08028 Barcelona, Spain*
[b] *Instituto de Catálisis y Petroleoquímica, C.S.I.C., Cantoblanco, 28049 Madrid, Spain*

Received 2 April 1996; accepted 9 August 1996

Abstract

Platinum–tin catalysts supported on either silica or γ-alumina have been prepared from $[PtCl(SnCl_3)(PPh_3)_2]$ bimetallic complex. The evolution of surface species under hydrogen from 473 to 873 K has been studied by in situ FTIR spectroscopy, mass spectrometry analysis of products evolved, X-ray diffraction (XRD), transmission electron microscopy (TEM), energy dispersive X-ray analysis (EDX), electron nanodiffraction, and X-ray photoelectron spectroscopy (XPS). The genesis of supported PtSn alloy as the only metallic phase on surface is shown for both supports. Catalytic performance and catalyst stability on the reaction between CO_2, C_2H_4 and H_2O to give lactic acid is reported. The characteristics of silica-supported catalysts contrast with those of alumina-supported ones.

Keywords: PtSn catalyst; Supported PtSn alloy; Activation of CO_2

1. Introduction

Many studies have been devoted to the development of new preparation methods for supported Pt–Sn bimetallic catalysts, due to their industrial importance and the complexity of the system. The preparation method and precursor used determine the characteristics of the final catalyst, including factors such as the extent of Pt–Sn alloy formation and the degree of tin reduction.

The more conventional preparations involve precursors like H_2PtCl_6, $Pt(NH_3)_4(OH)_2$ and $SnCl_2$, and incipient wetness, successive or co-impregnation methods [1,2]. However, others such as sol–gel methods [3], solvated metal atom dispersion techniques [4] or different methods based on the use of organometallic compounds [5–7] have also been used. The decomposition of surface organometallic compounds [5] and the preparation of catalysts from organometallic complexes via controlled surface reactions [6,7] have been widely used to improve control of the final characteristics of the catalysts. Among all these different possibilities,

* Corresponding authors. Fax: +34-3-4907725.

PII S1381-1169(96)00378-0

the use of bimetallic Pt–Sn compounds as metallic precursors is an attractive way of preparing supported platinum–tin bimetallic catalysts [8], particularly when the Pt–Sn interaction occurs in the molecular entity and is preserved during the anchoring process [9].

We have previously studied the heterogenization of $[PtCl(SnCl_3)(PPh_3)_2]$ complex on silica, its use as a catalyst in the hydroformylation reaction and its carbon dioxide activation capabilities [10,11]. Recently, we have reported the preparation of the single silica-supported PtSn alloy from $[PtCl_2(PPh_3)_2]$ and $SnCl_2$ [12]. Here we study the evolution of the $[PtCl(SnCl_3)(PPh_3)_2]$ heterogenized on silica or alumina during a reduction process under hydrogen from 473K to 873 K. The catalysts have been characterized by X-ray diffraction (XRD), transmission electron microscopy (TEM), energy dispersive X-ray analysis (EDX), electron nanodiffraction, and X-ray photoelectron spectroscopy (XPS). The formation and evolution of only the well defined silica- (or alumina-) supported PtSn alloy was shown during the process, although on alumina-supported catalysts chloride and phosphorus species from ligands were not fully eliminated during the reduction process. A support effect on the catalytic performance and catalyst stability of both the silica- and alumina-supported catalysts in the CO_2 reaction with C_2H_4 and H_2O to give lactic acid is reported.

2. Experimental

2.1. Preparation of catalysts

Two series of catalysts were prepared by anchoring *cis*-$[PtCl(SnCl_3)(PPh_3)_2]$ on silica and alumina carriers. The supports used were a Degussa Aerosil-type silica with a BET surface area of 200 $m^2 g^{-1}$ and a Girdler γ-alumina with a BET surface area of 188 $m^2 g^{-1}$ and a pore volume of 0.39 $cm^3 g^{-1}$. The complex *cis*-$[PtCl(SnCl_3)(PPh_3)_2]$ was prepared and characterized according to literature methods [13]. All chemicals used were of analytical reagent grade. Solvents were distilled, kept under argon and stored over activated molecular sieves.

Catalyst preparation was carried out in a single impregnation step from a methylene chloride solution of the complex on the supports, which were previously partially dehydrated by treatment under high vacuum at 473 K for 16 h. The anchoring of the complex was accomplished by treating the impregnates under high vacuum at 373 K overnight. All samples were prepared with a 3% platinum loading. Individual samples were reduced separately with hydrogen flow (40 $ml\,min^{-1}$) for 16 h at four different temperatures: 473, 573, 673 and 873 K. The resulting catalysts are referred to as $PtSn/SiO_2T$ or $PtSn/Al_2O_3T$, where T indicates the reduction process temperature in kelvin.

2.2. Characterization of catalysts

2.2.1. Infrared spectroscopy

Samples for IR experiments were prepared in situ by adsorption of the metallic precursor solution onto carrier disks using vacuum-gasline and break-seal techniques. A special greaseless infrared cell with CaF_2 windows which allowed thermal treatments was used. Infrared spectra were recorded on a Nicolet 520 Fourier transform spectrophotometer working with a resolution of 2 cm^{-1}. The products evolving during the reduction processes were characterized by GC-MS in a Hewlett Packard 5890 instrument equipped with a 5971 mass-selective detector.

2.2.2. Transmission electron microscopy

Samples for TEM studies were placed on carbon-coated copper grids from methanol suspensions. Bright-field and dark-field studies were carried out using a Hitachi H 800-MT transmission electron microscope operating at 175 keV. EDX measurements were performed

in STEM mode with a Kevex 8000 Quantum System and a 10 nm probe in the range 0–10 keV. Electron diffraction studies were carried out using a Hitachi H 800-NA transmission electron microscope operating in the convergent beam mode at 200 keV with a 2–5 nm probe.

2.2.3. X-ray diffraction

X-ray diffraction patterns of powders were collected using a Siemens D-500 X-ray diffractometer equipped with a graphite monochromator and a Cu target at a step width of 0.02 degrees and by counting 10 s at each step. The average particle size was estimated using the Scherrer formula at various high-intensity reflections corrected from CuKα2 radiation.

2.2.4. Photoelectron spectroscopy

Photoelectron spectra were acquired with a Fisons ESCALAB 200 R spectrometer equipped with a hemispherical electron analyzer and Mg Kα X-ray source (1253.6 eV). The samples were mounted on a sample rod placed in a pretreatment chamber, and reduced in-situ in hydrogen at different temperatures (473, 573, 673 and 873 K) for 1h. The base pressure in the ion-pumped analysis chamber was maintained below 2×10^{-9} Torr (1 Torr = 133.3 N/m^2) during data acquisition. For each sample, C 1s, Si 2p (or Al 2p), Sn 3d, Pt 4f, Cl 2p and P 2p peaks were recorded working at a pass energy of 10 eV). The intensities were estimated by calculating the integral of each peak after subtraction of the 's'-shaped background and fitting the experimental curve to a mixture of Lorentzian and Gaussian lines of variable proportion [14]. The binding energies were calculated using the Si 2p peak at 103.4 eV or the Al 2p at 74.7 eV. The accuracy of the BE values was within ± 0.2 eV.

2.3. Catalytic activity

The catalytic experiments were carried out in a stainless steel continuous flow microreactor operating under differential conditions. High purity carbon dioxide and ethylene were supplied from a pressurized manifold via individual mass flow controllers. Bi-distilled water was introduced into the reactant mixture by a mechanical pump equipped with a 'varispeed device'. Reaction products were sampled on-line through an automated gas sample valve into a Varian 3400 gas chromatograph. A DB5 capillary column connected to a flame ionization detector, and a Hayesep column and a 5 Å molecular sieve column connected to a thermal conductivity detector were used to analyze the reaction products. The transfer line between the reactor and the gas chromatograph and all valves in the chromatograph were coated with fused silica and heated above 423 K in order to eliminate any product loss. A complete analysis of the products was made by collecting them in a solid CO_2 trap at the reaction outlet and analyzing them by GC-MS using a Hewlett Packard 5971 mass selective detector.

3. Results and discussion

The chemical route for the heterogenization of $[PtCl(SnCl_3)(PPh_3)_2]$ on silica had been reported elsewhere [10]. A similar method was used to anchor this complex on alumina. The next step was to examine the evolution of surface species under reduction conditions. To this end, in situ FTIR spectroscopy, mass spectrometry analysis of products evolved and in situ XPS analysis were applied, and the catalysts were characterized after each reduction step (473, 573, 673 and 873 K) by XRD, TEM, EDX and electron nanodiffraction techniques.

3.1. Characterization of catalysts

After H_2-reduction at 473 K, the silica-supported sample led to the formation of a hydride complex characterized by a vibration mode ν(Pt–H) at 2132 cm^{-1}, which was evidenced by in situ infrared spectroscopy. Simultaneously, the evolution of hydrogen chloride was

observed by mass spectrometry. After 16 h of treatment under hydrogen at 473 K TEM analysis of the silica-supported sample showed the formation of a fibrous surface structure on which small metallic nuclei about 8 nm in diameter were evidenced (see Fig. 1a), for which different EDX analyses on the fibrous structure only showed platinum and tin. The XRD pattern for this sample (Fig. 2, pattern a) was assigned unambiguously to the hcp PtSn alloy, and no

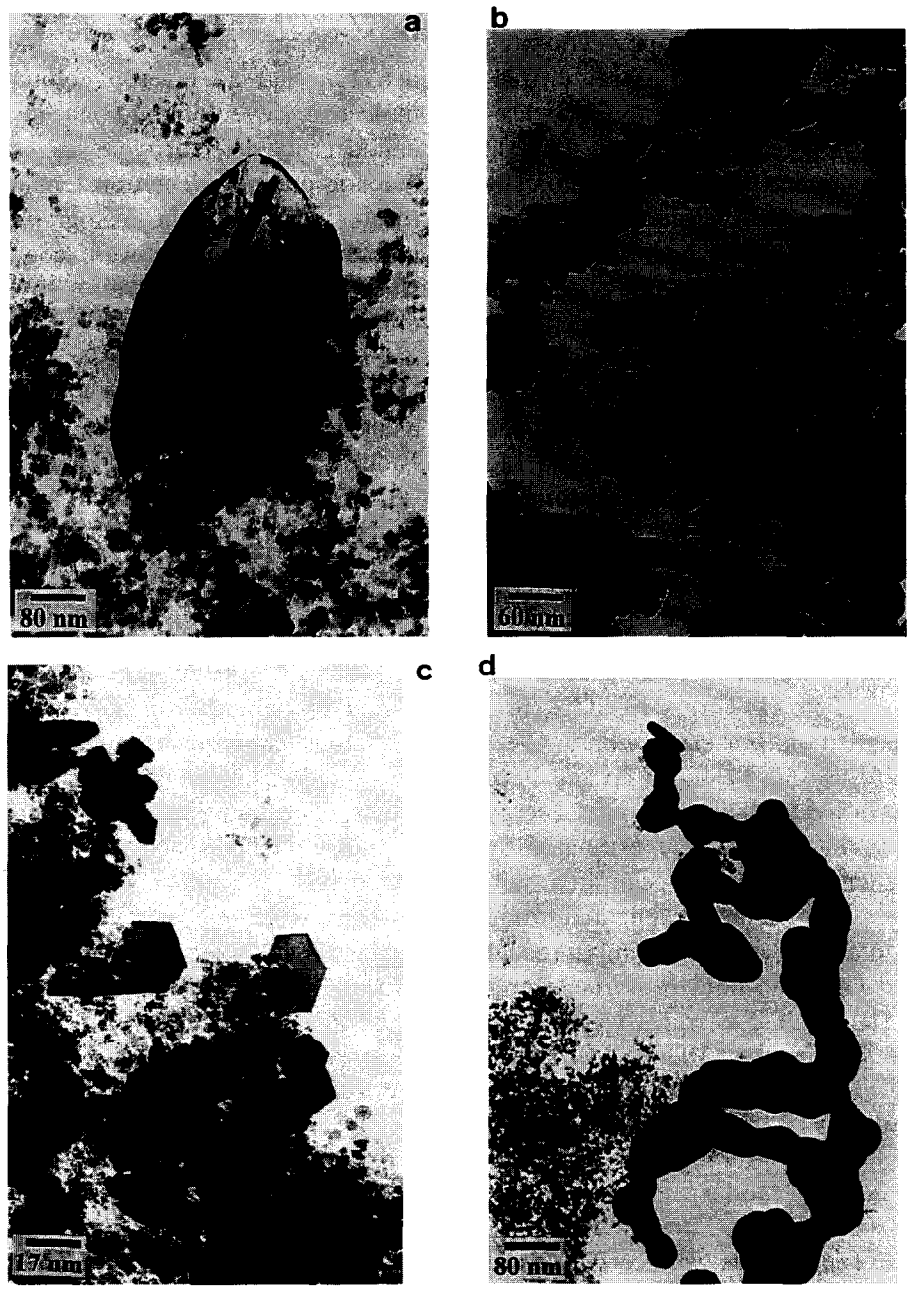

Fig. 1. TEM micrographs of the silica-supported samples after 16 h under hydrogen at different temperatures (T), $PtSn/SiO_2T$. (a) $PtSn/SiO_2473$. (b) $PtSn/SiO_2573$. (c) $PtSn/SiO_2673$. (d) $PtSn/SiO_2873$.

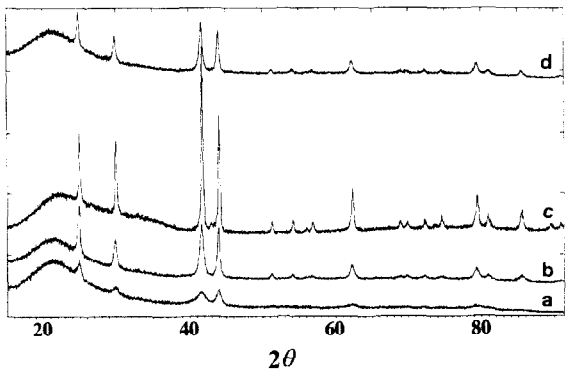

Fig. 2. XRD patterns of the silica-supported samples with the temperature (T) of the hydrogen treatment (16 h), $PtSn/SiO_2T$. $a = PtSn/SiO_2473$; $b = PtSn/SiO_2573$; $c = PtSn/SiO_2673$; $d = PtSn/SiO_2873$.

other mono- or bimetallic phases could be discerned by this technique.

XP spectra of the samples corresponding to Si 2p, Pt 4f, Sn 3d and Cl 2p core levels were recorded. High-resolution Pt 4f and Sn 3d core-level spectra for silica-supported samples are shown in Fig. 3A and B, respectively. By applying peak synthesis procedures, the Sn $3d_{5/2}$ peak could be fitted to three components in all catalysts, while the Pt 4f doublet was fit to one component, except for the $PtSn/SiO_2473$ which was fitted to two doublets. For the $PtSn/SiO_2473$ sample (Fig. 3A, spectrum a), the presence of Pt^0 and Pt(II) species was observed (see Table 1) ($Pt^0/Pt_{total} = 0.83$). The Sn 3d doublet is much more complex, and, for the sake of clarity only the Sn $3d_{5/2}$ peak will be considered instead the two peaks of the doublet. The Sn $3d_{5/2}$ peak shows three components (Fig. 3B): ca. 483.6 eV attributed to Sn^0, at ca. 485.0 assigned to Sn in a PtSn alloy (Sn^0_{al}) and

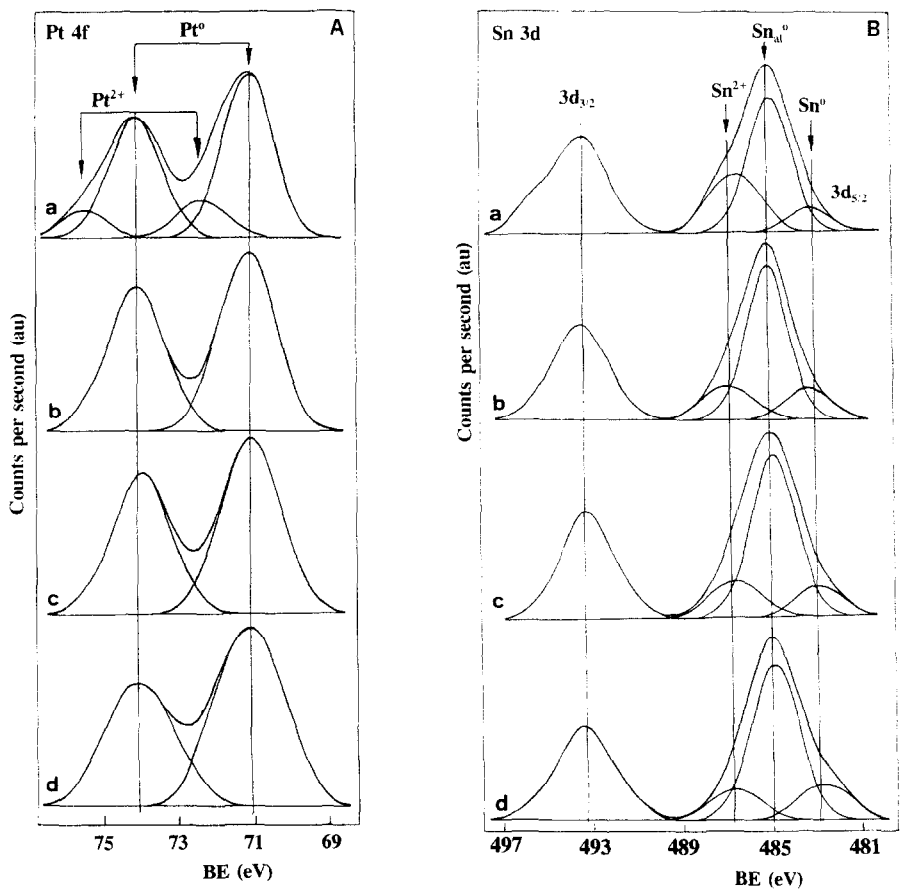

Fig. 3. XP spectra corresponding to the *Pt 4f* (A) and *Sn 3d* (B) levels of the silica-supported samples after hydrogen treatment (16 h) at different temperatures, $PtSn/SiO_2T$. $a = PtSn/SiO_2473$; $b = PtSn/SiO_2573$; $c = PtSn/SiO_2673$; $d = PtSn/SiO_2873$.

Table 1
Binding energies (eV) of core electrons of the atoms for the silica-supported PtSn catalysts [a]

Catalyst	Pt $4f_{7/2}$ [b]	Sn $3d_{5/2}$ [b]	Cl $2p_{3/2}$
$PtSn/SiO_2$473	71.1 (83)	483.6 (10)	198.2
	72.5 (17)	484.9 (55)	
		486.8 (35)	
$PtSn/SiO_2$573	71.2	483.6 (16)	198.5
		484.9 (66)	
		486.8 (18)	
$PtSn/SiO_2$673	71.1	483.5 (16)	—
		485.0 (62)	
		486.9 (22)	
$PtSn/SiO_2$873	71.2	483.6 (21)	—
		485.2 (62)	
		486.8 (17)	

[a] The C1s peak at a binding energy of 284.9 eV was taken as an internal standard. A value of 103.4 eV was obtained for the Si 2p peak in all experiments.
[b] Values in parentheses indicate the relative percentage of surface species for each sample.

ca. 486.8 eV attributed to Sn^{2+}. It can be noted that most of the XPS studies reported in literature allow determination of the chemical state of both Pt and Sn but the data do not permit definition of whether Sn^0 is in the form of a PtSn alloy. Fortunately, this uncertainty has been excluded in the present work due to catalysts single-phase content and analyses high resolution conditions. Following Wagner et al. [15] the relative atomic ratios on the surface were calculated from the relative intensities of the peaks to the Si 2p peak and the sensitivity factors (see Table 2). An enrichment of tin species at the surface relative to platinum species can be inferred. Table 2 summarizes the atomic ratios relative to the silicon peak, some residual chlorine species can be inferred for $PtSn/SiO_2$473 catalyst and to a lesser extent for the $PtSn/SiO_2$573 catalyst.

After treatment under hydrogen at 573 K, the triphenylphosphine ligands were fully eliminated as evidenced by infrared spectroscopy, and the formation of PtSn metallic nuclei was confirmed. Fig. 2 shows the evolution of the XRD pattern for the silica-supported sample as a function of the hydrogen treatment temperature. Only the XRD profile of PtSn alloy can be seen at any hydrogen treatment temperature up to 873 K.

In Fig. 1b, c and d TEM micrographs corresponding to different silica-supported samples after hydrogen treatments at 573, 673 and 873 K are shown. The formation of hexagonal particles after hydrogen treatment at 573 K (see $PtSn/SiO_2$573 micrograph, Fig. 1b) and specifically after hydrogen treatment at 673 K (see $PtSn/SiO_2$673 micrograph, Fig. 1c) is clearly visible. The PtSn particles in samples $PtSn/SiO_2$573 and $PtSn/SiO_2$673 have a plate-like structure, as inferred from TEM observations and XRD measurements. XRD patterns of these samples exhibit a strong textural effect, the line profiles of (hk0) peaks (2θ at 44°) are especially narrow in comparison to other reflections, thus indicating the presence of metallic particles with a platelet morphology on a basal plane perpendicular to the [001] direction.

The nature of these particles was confirmed by multiple EDX analysis and electron nanodiffraction patterns. All EDX analyses only showed Pt and Sn and the electron nanodiffraction experiments gave patterns which corresponded well to the PtSn alloy with hcp structure. The electron nanodiffraction pattern (Fig. 4a) and the indexed pattern (Fig. 4b) corresponding to a representative individual particle of $PtSn/SiO_2$573 show the (hcp) structure oriented in the [0001] crystallographic direction.

The increase in temperature up to 873 K produced a sintering of silica-supported PtSn particles, but no segregation of any other phase was observed by TEM (Fig. 1d) or XRD (Fig. 2, pattern d). In the XRD profile of this sample

Table 2
Surface atomic ratios (XPS) for the silica-supported PtSn catalysts

Catalyst	Pt/Si_{at}	Sn/Si_{at}	Pt/Sn_{at}	Cl/Si_{at}
$PtSn/SiO_2$473	0.0304	0.0587	0.94	0.0163
$PtSn/SiO_2$573	0.0265	0.0490	0.82	0.0016
$PtSn/SiO_2$673	0.0090	0.0196	0.74	traces
$PtSn/SiO_2$873	0.0084	0.0168	0.81	—

the (hk0) reflections no longer have distintive width, thus indicating a sintering of the particles in all directions.

Table 3 summarizes the crystal size of supported PtSn particles for all catalysts prepared. For silica-supported samples it was possible to find crystal size values from TEM and XRD patterns, and a good agreement between them was observed. EDX patterns for all the silica-supported samples treated from 473 to 873 K showed similar platinum-to-tin peak ratios, as expected from the invariant composition of metallic particles during the reduction process.

XP spectra for samples treated at 573 K or higher show in all cases only metallic Pt species (Fig. 3A) and the three tin species, i.e., Sn^{2+}, Sn^{0}_{al} and Sn^{0} (Fig. 3B). The relative atomic ratios on the surface shown in Tables 1 and 2 indicate a segregation of tin on the surface, which has a high reduction degree.

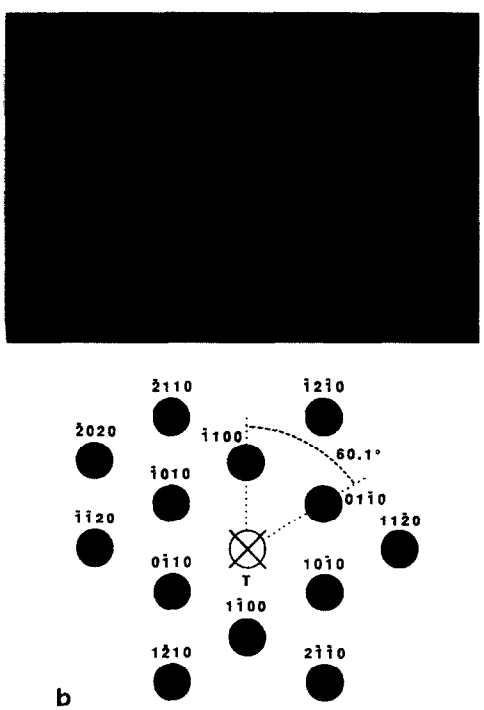

Fig. 4. (a) Electron nanodiffraction pattern coorresponding to a representative particle of $PtSn/SiO_2$573 sample. (b) Indexed nanodiffraction pattern shown in (a). The particle has the PtSn (hcp) structure oriented in the [0001] crystallographic direction.

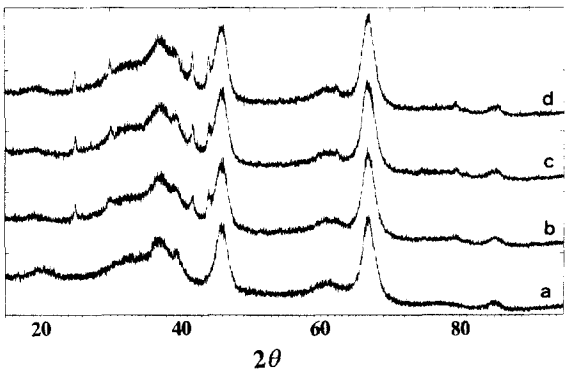

Fig. 5. XRD patterns of the alumina-supported samples with the temperature (T) of the hydrogen treatment (16 h), $PtSn/Al_2O_3T$. a = $PtSn/Al_2O_3$473; b = $tSn/Al_2O_3$573; c = $PtSn/Al_2O_3$673; d = $PtSn/Al_2O_3$873.

The $[PtCl(SnCl_3)(PPh_3)_2]$ complex was anchored on alumina carrier in a similar manner as on silica, and aliquots of the supported precursor were reduced in H_2 at temperatures from 473 to 873 K. Fig. 5 displays the XRD patterns for alumina-supported samples reduced at different temperatures. Only the presence of alumina-supported PtSn alloy is observed by this technique; this phase is seen after a reduction process at 573 K.

In Fig. 6 TEM micrographs obtained for each sample are shown. For $PtSn/Al_2O_3$473 sample spherical aggregates (125–312 nm diameter) can be seen (Fig. 6a), which evolve to smaller hexagonal particles after treatment under hydrogen at 573 and 673 K (Fig. 6b and c). As occurs

Table 3
Particle size of silica- or alumina-supported PtSn alloy determined from TEM and XRD

Catalyst	PtSn particle size (nm)	
	TEM	XRD
$PtSn/SiO_2$473	8	12
$PtSn/SiO_2$573	20×5 [a]	21 [b]
$PtSn/SiO_2$673	25×6 [a]	27 [b]
$PtSn/SiO_2$873	59	57
$PtSn/Al_2O_3$573	14×3 [a]	—
$PtSn/Al_2O_3$673	17×4 [a]	—
$PtSn/Al_2O_3$873	31	—

[a] Values expressed as $A \times B$, where A indicates the basal plane direction and B the c axis direction.
[b] Values corresponding to the basal plane direction.

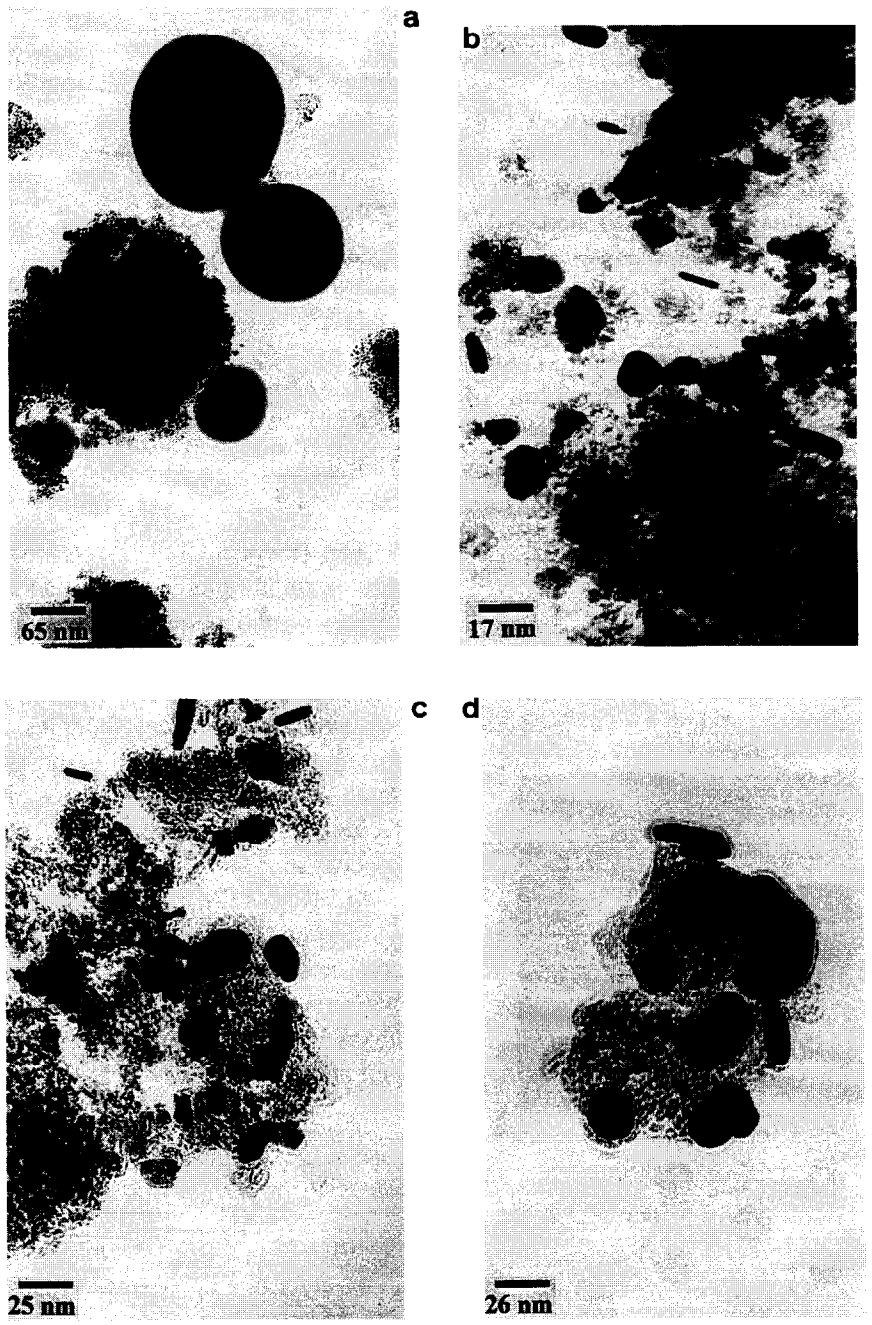

Fig. 6. TEM micrographs of the alumina-supported samples after 16 h under hydrogen at different temperatures (T). PtSn/$Al_2O_3$$T$. (a) PtSn/$Al_2O_3$473. (b) PtSn/$Al_2O_3$573. (c) PtSn/$Al_2O_3$673. (d) PtSn/$Al_2O_3$873.

in silica-supported samples, an increase in temperature up to 873 K led to sintering of PtSn alloy particles and no segregation of other phases was observed. At a given temperature, PtSn particles generated on alumina were smaller than those generated on silica (see Table 3). EDX analysis of alumina samples treated from 573 to 873 K showed similar platinum-to-tin

peak ratios, which also agrees with the similar composition of metallic particles produced during the reduction process.

Photoelectron spectroscopy provides additional information. In Fig. 7 XP spectra of the Pt 4f (Fig. 7A) and Sn 3d (Fig. 7B) levels for alumina-supported samples are presented. Because the Al2p peak of the alumina overlaps with the Pt 4f peaks, a curve synthesis procedure was carefully performed assuming an intensity ratio of Pt $4f_{7/2}$ to Pt $4f_{5/2}$ of 1:0.75. Table 4 compiles Pt $4f_{7/2}$, Sn $3d_{5/2}$, Cl $2p_{3/2}$ and P 2p binding energies of core electrons corresponding to alumina-supported samples. From these XP data for the alumina-supported catalysts, no complete removal of chlorine and phosphorus species coming from the ligands of $[PtCl(SnCl_3)(PPh_3)_2]$ precursor had occurred. Binding energies of Cl $2p_{3/2}$ corresponded well for all alumina catalysts to the presence of surface chloride species. On the other hand surface phosphorus species developed along with the reduction process. After reduction at 473 K, phosphine (P 2p binding energy 130.7

Table 4
Binding energies (eV) of core electrons of the atoms for the alumina-supported PtSn catalysts [a]

Catalyst	Pt $4f_{7/2}$	Sn $3d_{5/2}$ [b]	Cl $2p_{3/2}$	P 2p [b]
$PtSn/Al_2O_3473$	71.2	485.3 (43)	198.6	130.7(43)
		487.0 (57)		132.5(57)
$PtSn/Al_2O_3573$	71.3	483.9 (20)	198.7	134.1
		484.8 (52)		
		486.9 (28)		
$PtSn/Al_2O_3673$	71.2	483.7 (21)	198.7	134.1
		484.8 (35)		
		487.0 (44)		
$PtSn/Al_2O_3873$	71.2	483.4 (18)	198.9	134.3
		484.6 (35)		
		486.7 (47)		

[a] The C 1s peak at a binding energy of 284.9 eV was taken as an internal standard. A value of 74.5 eV was obtained for the Al 2p peak in all experiments.
[b] Values in parentheses indicate the relative percentage of surface species for each sample.

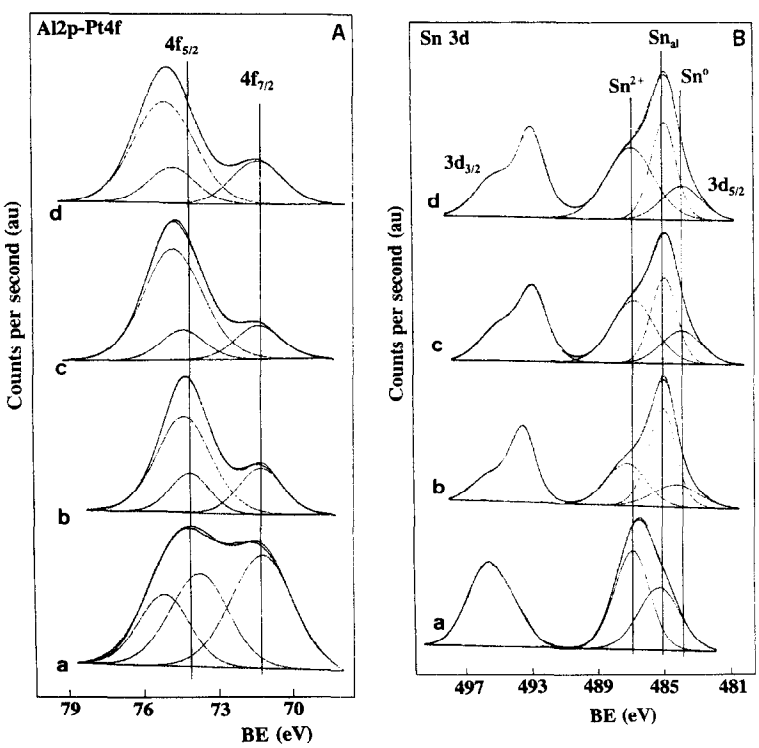

Fig. 7. XP spectra corresponding to the *Pt 4f* (A) and *Sn 3d* (B) levels of the alumina-supported samples after hydrogen treatment (16 h) at different temperatures, $PtSn/Al_2O_3T$. *a* = $PtSn/Al_2O_3473$; *b* = $PtSn/Al_2O_3573$; *c* = $PtSn/Al_2O_3673$; *d* = $PtSn/Al_2O_3873$.

Table 5
Surface atomic ratios (XPS) for the alumina-supported PtSn catalysts

Catalyst	P/Al_{at}	Cl/Al_{at}	Pt/Al_{at}	Pt/Sn_{at}
$PtSn/Al_2O_3473$	0.104	0.198	0.145	0.66
$PtSn/Al_2O_3573$	0.031	0.025	0.028	0.88
$PtSn/Al_2O_3673$	0.028	0.022	0.017	0.74
$PtSn/Al_2O_3873$	0.035	0.010	0.026	0.67

Table 6
Lactic acid production over $PtSn/SiO_2673$ from CO_2, C_2H_4 and H_2O [a]

T (K)	373	393	423	423	423	473
P (bar)	35	35	25	30	35	35
μmol lactic acid min^{-1} g^{-1} cat.	4	23	2	47	90	20

[a] Molar ratio CO_2:C_2H_4:H_2O = 1:1:1; catalyst charge 0.9 g; 10^{-2} total mol reactants min^{-1} g^{-1} catalyst.

eV) and phosphonium (P 2p binding energy 132.5 eV) species were observed at the catalyst surface. These species evolved to phosphate (P 2p binding energy 134.3 eV) species after a treatment at 573 K, probably by interaction with OH groups of γ-alumina. The binding energy of Pt $4f_{7/2}$ indicates in all cases the presence of surface Pt^0 species. A peak synthesis procedure applied to Sn 3d XP spectra again showed the presence of oxidized tin, and two types of reduced tin: One of them similar to that found on silica supported catalysts, assigned to Sn alloyed with Pt, and the other one, less abundant, with smaller values of binding energies, due to metallic tin. Table 5 displays surface atomic ratios relative to the alumina peak, a significant content of surface chloride and phosphorus species and a tin segregation relative to platinum can be inferred.

3.2. Catalytic activity

The coupling catalytic reaction between CO_2, C_2H_4 and H_2O was studied on $PtSn/SiO_2673$ and $PtSn/Al_2O_3673$ catalysts at 25 to 35 bar total pressure and in the temperature range 373–473 K. We had reported the production of lactic acid in these conditions over a catalyst prepared from monometallic precursors but with the single PtSn bimetallic phase on silica [12].

Results of lactic acid production over $PtSn/SiO_2673$ catalyst are shown in Table 6. This catalyst with the single PtSn phase supported on silica showed comparable activity values to those already reported, which had similar composition [12]. The resistance to aging of this $PtSn/SiO_2673$ catalyst is remarkable; after running under reaction conditions for three weeks the characteristics of the catalyst were unchanged, as evidenced by XRD, TEM and catalytic activity values. Only silica-supported PtSn particles were observed, whose size and morphology were essentially unchanged after reaction.

In contrast, $PtSn/Al_2O_3673$ catalyst showed no activity in this reaction and no lactic acid was obtained with any reaction conditions used. In spite of the similar Sn 3d and Pt 4f features for the catalysts supported either on silica or on alumina it appears that the role of γ-alumina as support determines its final characteristics. The interaction of the ligands of the catalyst precursor with the surface of γ-alumina prevents its complete removal during the reduction process, and the presence of chloride and phosphate species on the surface are evidenced after any hydrogen treatment to 873 K. At the end of the catalytic run the $PtSn/Al_2O_3673$ catalyst was treated with an aqueous solution of HCl, and after CH_3OH addition, the presence of the methyl esther of lactic acid was observed in the solution. The possibility of formation of lactic

Fig. 8. TEM micrograph of $PtSn/Al_2O_3673$ sample after reaction.

acid on the PtSn phase supported on alumina cannot be ruled out, although it may remain strongly adsorbed on the highly basic surface species mentioned above. Moreover, significant morphological changes seem to occur in $PtSn/Al_2O_3673$ catalyst under reaction conditions. The TEM micrograph of $PtSn/Al_2O_3673$ catalyst after reaction is shown in Fig. 8. Metallic particles no longer have platelet morphology, and the destruction of initial alumina-supported PtSn particles is observed. Besides the segregation of small platinum particles indicated by EDX, sintered bimetallic aggregates can also be observed.

4. Conclusions

Silica and alumina supported bimetallic PtSn catalysts have been prepared by anchoring the precursor $[PtCl(SnCl_3)(PPh_3)_2]$ bimetallic complex. After hydrogen treatments at temperatures in the range 473–873 K a bimetallic PtSn alloy was developed at the catalyst surface. The genesis of this alloy was monitored by in situ FTIR spectroscopy, X-ray diffraction, transmission electron microscopy, energy dispersive X-ray analysis, electron nanodifraction and photoelectron spectroscopy. Due to its high surface sensitivity, photoelectron spectroscopy revealed not only the PtSn alloy but also a variable proportion of both unreduced Sn^{2+} and reduced Sn^0 species, depending on the temperature of reduction. The PtSn alloy was found to be active in the coupling reaction of CO_2 with ethylene and water to form lactic acid. While the yields were moderately high on the silica carrier, on alumina carrier a strong adsorption of the products on the basic sites, produced through phosphine degradated fragments, blocked catalyst activity.

Acknowledgements

We thank DGICYT (MAT 93-0477) and CIRIT (INU 93) for financial support and the Serveis Científico-Tècnics UB for chemical analysis and apparatus facilities.

References

[1] R. Srinivasan, L. Rice and B.H. Davis, J. Catal. 129 (1991) 257.
[2] K. Balakrishnan and J. Schwank, J. Catal. 127 (1991) 287.
[3] R. Gómez, V. Bertin, M.A. Ramírez, T. Zamudio, P. Bosch and I. Shifter, T. López, J. Non-Cryst. Solids 110 (1989) 170.
[4] Y.X. Li and K.J. Klabunde, J. Catal. 126 (1990) 173.
[5] Y.I. Yermakov and B.N. Kuznetsov, J. Mol. Catal. 9 (1980) 13.
[6] E. Kern-Tálas, M. Hegedüs, S. Göbölös, P. Szedlacsek, and V. Margitfalvi, in: B. Delmon, P. Grange, P.A. Jacobs and G. Poncelet (Editors), Sud. Surf. Sci. Catal. 31 (1987) 689.
[7] J.-P. Candy, B. Didillon, E.L. Smith, T.B. Shay and J.-M. Basset, J. Mol. Catal. 86 (1994) 179.
[8] C. Kappenstein, M. Saouabe, M. Guérin, P. Marecot, I. Uszkurat and Z. Paal, Catal. Lett. 31 (1995) 9.
[9] S.R. de Miguel, G.T. Baronetti, A.A. Castro and O.A. Scelza, Appl. Catal. 45 (1988) 61.
[10] N. Homs, N. Clos, G. Muller, J. Sales, P. Ramirez de la Piscina and J.L.G. Fierro, J. Mol. Catal. 74 (1992) 401.
[11] J. Llorca, P. Ramirez de la Piscina, J. Sales and N. Homs, J. Chem. Soc., Chem. Commun. (1994) 2555.
[12] J. Llorca, P. Ramirez de la Piscina, J.L.G. Fierro, J. Sales and N. Homs, J. Catal. 156 (1995) 139.
[13] P.S. Pregosin and S.N. Sze, Helv. Chim. Acta 61 (1978) 1848.
[14] D.A. Shirley, Phys. Rev. 35 (1972) 4909.
[15] C.D. Wagner, L.E. Davis, M.V. Zeller, J.A. Taylor, R.H. Raymond and L.H. Gale, Surf. Interface Anal. 3 (1981) 211.